Thermal diffusion behavior of hard sphere suspensions

Hui Ning,[1,*] Johan Buitenhuis,[1,†] Jan K. G. Dhont,[1,‡] and Simone Wiegand[1,§]

[1]*Forschungszentrum Jülich GmbH,*

IFF - Weiche Materie, D-52428 Jülich, Germany

(Dated: November 2, 2006)

Abstract

We studied the thermal diffusion behavior of octadecyl coated silica particles (R_h = 27 nm) in toluene between 15.0°C and 50.0°C in a volume fraction range of 1% to 30% by means of thermal diffusion forced Rayleigh scattering. The colloidal particles behave like hard spheres at high temperatures and as sticky spheres at low temperatures. With increasing temperature, the obtained Soret coefficient S_T of the silica particles changed sign from negative to positive, which implies that the colloidal particles move to the warm side at low temperatures, whereas they move to the cold side at high temperatures. Additionally, we observed also a sign change of the Soret coefficient from positive to negative with increasing volume fraction. This is the first colloidal system for which a sign change with temperature and volume fraction has been observed. The concentration dependence of the thermal diffusion coefficient of the colloidal spheres is related to the colloid-colloid interactions, and will be compared with an existing theoretical description for interacting spherical particles. To characterize the particle-particle interaction parameters, we performed static and dynamic light scattering experiments. The temperature dependence of the thermal diffusion coefficient is predominantly determined by single colloidal particle properties, which are related to colloid-solvent molecule interactions.

PACS numbers: 66.10.Cb, 83.80.Hj

I. INTRODUCTION

Colloidal particles are small enough to exhibit thermal motion commonly referred to as Brownion motion. Being just very large molecules in solvent, colloidal particles show many physical phenomena that are also found in ordinary molecular systems. Consequently, colloids have been used frequently to study fundamental questions in physics. Therefore, it is expected that they are also a suitable model system to illuminate the microscopic mechanism underlying the Ludwig-Soret effect, which was discovered already 150 years ago.[1,2] This effect, also known as thermal diffusion, describes the diffusive mass transport induced by a temperature gradient in a multi-component system. In a binary fluid mixture with non-uniform concentration and temperature, the mass flow J_m of component 1 contains contributions stemming from gradients in concentration *and* in temperature,

$$J_m = -\rho D \nabla w - \rho w(1-w) D_{\mathrm{T}} \nabla T \tag{1}$$

Here ρ is the mass density of the homogeneous mixture, D is the translational diffusion coefficient, w is the weight fraction of component 1 and D_{T} is the thermal diffusion coefficient. The Soret coefficient S_{T} is defined as $S_{\mathrm{T}} \equiv D_{\mathrm{T}}/D$, which is proportional to the ratio of the concentration- and temperature-gradient in the stationary state

$$S_T = -\frac{1}{w(1-w)} \frac{\mid \nabla w \mid}{\mid \nabla T \mid}. \tag{2}$$

A number of studies show that interactions play an important role for the thermal diffusion behavior, where long ranged repulsion between charged micelles and colloids have been considered.[3–5]

Conceptually, thermal diffusive behavior of *highly diluted* and *concentrated* solutions can be differentiated. In dilute solutions, where colloid-colloid interactions can be neglected, the thermal diffusion coefficient of the colloids is determined by the nature of the interactions between single colloidal particles and solvent molecules (and possibly other solutes like ions that form a double layer around the colloids). Structural changes of the surrounding solvation layer due to temperature changes and/or changes of the solvent composition may induce a sign change of the thermal diffusive behavior of single colloidal particles. One example is the sign change of Soret coefficient of poly(ethylene oxide) in ethanol/water as function of the solvent composition.[6] Here, a sign change is observed at a weight fraction of water

where hydrogen bonds break by adding ethanol. For concentrated solutions, colloid-colloid interactions affect the thermal diffusive behavior of the colloidal particles. A pronounced concentration dependence of the Soret coefficient has been found in experiments[3,7] and is predicted by theory.[8,9]

In recent years, modern optical techniques have been developed which allow the investigation of complex fluids with slow dynamics such as polymer solutions and blends, micellar solutions, colloidal dispersions and bio-molecules.[5,10–15] The main issues of interest were the derivation of scaling laws and to understand the sign change of the Soret coefficient for macromolecular and colloidal systems on the basis of existing theories for molecular fluids.

In the past few years several theoretical concepts have been proposed to understand single particle and colloid-colloid interaction contributions to the thermophoretic motion of colloidal particles.[8,9,16–19] Bringuier and Bourdon proposed a relation between the Soret coefficient in terms of a mean-field potential energy, which gives in principle access to both the single-particle as well as the colloid-colloid interaction contributions. In rare cases for which the mobility of the particle is known, a comparison with experimental data is possible. While the majority of the theoretical approaches give expressions for the single particle contribution, the work by Dhont gives explicit expressions for the contribution of colloid-colloid interactions to the thermal diffusion coefficient D_{T}. These interaction contributions lead to a concentration dependence of the thermal diffusion coefficient. According to this theory, a sign change of the Soret coefficient as a function of temperature and concentration is possible for appropriate interaction parameters.

This paper is concerned with experiments on thermal diffusion of a colloidal hard-sphere model system. The experimental data will be compared to the above mentioned theoretical predictions for hard spheres. This paper is organized as follows: in Section II, we will summarize the relevant part of theory by Dhont. In Section III we briefly describe the experimental details and summarize the working equations. In Section IV, we will present thermal diffusion forced Rayleigh scattering (TDFRS) and light scattering (DLS and SLS) results. Finally, the results from experiments are compared to theory as far as the interaction contributions are concerned.

II. THEORY

A. The interaction potential between colloids

The interaction between silica particles coated with octadecyl chains in various organic solvents has been extensively studied.[20–23] The same type of colloidal particles are used in the present study. At low temperatures, the octadecyl chains grafted to the surface of the colloidal particles give rise to a very short-ranged, attractive interaction potential. The range of the attractive component of the interaction potential is very much smaller as compared to the size of the core of the colloids. At high temperatures, the depth of the attractive potential vanishes, where the colloids interact through a hard-core potential.

The interaction potential at lower temperatures for such "sticky spheres" can be written as,

$$V(R|T) = \begin{cases} \infty & \text{for } R < 2a \\ \epsilon(T)\frac{R-2a-\Delta}{\Delta} & \text{for } 2a \leq R \leq 2a+\Delta \\ 0 & \text{for } 2a+\Delta < R \end{cases} \tag{3}$$

where a is the radius of the colloidal spheres, R is the distance between the centers-of-mass of the spheres, ϵ is the depth of the attractive potential and Δ is the range of the attractive potential. The range Δ is approximately equal to the length 0.3 nm of the octadecane molecules. The depth ϵ of the attraction is in this case related to the quality of the solvent for the octadecyl brush. In particular, the depth of the attraction is temperature dependent, since the quality of the solvent changes with temperature. The temperature dependence of ϵ can be described by[20]

$$\epsilon(T) = \begin{cases} L(\frac{\theta}{T} - 1)k_B T & \text{for } T < \theta \\ 0 & \text{for } T \geq \theta \end{cases} \tag{4}$$

where L is proportional to the overlap volume fraction of two brushes and θ is the θ-temperature of the chain-solvent combination.

According to eq.(4) for the depth of the attraction, the potential (3) reduces to the hard-sphere potential above the θ-temperature,

$$V(R|T) = \begin{cases} \infty & \text{for } R \leq 2a \\ 0 & \text{for } R > 2a \end{cases} \tag{5}$$

The interaction parameters L and θ can be obtained from static and dynamic light

scattering. Static light scattering probes the second virial coefficient B_2,

$$B_2 \equiv \int_0^\infty (1 - exp(-\frac{V(R|T)}{k_B T}))r^2 dr = 4V_{\rm HS}[1 + \frac{3\Delta}{2a}F_D(\beta\epsilon)] , \quad (6)$$

where

$$F_D(\beta\,\epsilon) = (1 + \beta\epsilon - exp\{\beta\epsilon\})/\beta\epsilon , \quad (7)$$

with $\beta = 1/k_B T$ (k_B is Boltzmann's constant). For high temperatures, where $\beta\epsilon = 0$, this reduces to the well-known hard-sphere result $B_2 = 4\,V_{\rm HS}$, where $V_{\rm HS}$ is the volume of a colloidal particle. Dynamic light scattering probes the collective diffusion coefficient which is equal to[9]

$$D = D_0[1 + \phi(1.45 + 4.50\frac{3\Delta}{2a}F_D(\beta\,\epsilon))] , \quad (8)$$

in leading order of concentration. Here, ϕ is the volume fraction and D_0 is the Einstein translational diffusion coefficient of a non-interacting colloidal sphere.

B. Thermal diffusion of interacting colloids

According to the theory by Dhont,[9] the additive contribution to the interacting part of the thermal diffusion coefficient $D_{\rm T,int}^{\rm theo}$, which arises from colloid-colloid interactions, consists of two contributions,

$$D_{\rm T,int}^{\rm theo} = D_{\rm T}^{(0)} + D_{\rm T}^{(i)} , \quad (9)$$

where $D_{\rm T}{}^{(i)}$ accounts for a possible temperature dependence of the colloid-colloid pair-interaction potential, and $D_{\rm T}{}^{(0)}$ is the remaining contribution. The latter contribution is the only contribution that would remain in case the pair-potential would be temperature independent. It should be mentioned that $D_{\rm T,int}^{\rm theo}$ is related to the interaction contribution $D_{\rm T,int}$ to the thermal diffusion coefficient $D_{\rm T}$ defined in Eq. 1, as,

$$D_{\rm T,int} = V_c^0 D_{\rm T,int}^{\rm theo}/[\phi(1-\phi)] . \quad (10)$$

This relation is derived in the appendix. By integration of the Smoluchowski equation, it is found that,

$$D_{\rm T}^{(0)} = D_0\frac{\rho_{\rm N}}{T}[1 + \alpha_T^0\phi + \mathcal{O}(\phi^2)] , \quad (11)$$

and,

$$D_{\rm T}^{(i)} = D_0\frac{\rho_{\rm N}}{T}[\alpha_T^i\phi + \mathcal{O}(\phi^2)] , \quad (12)$$

where $\rho_{\rm N}$ is the number density of colloids, ϕ is the volume fraction of colloids, and α_T^0 and α_T^i are the leading-order virial coefficients for $D_{\rm T}^{(0)}$ and $D_{\rm T}^{(i)}$, respectively. The first term in Eqs.11 is the "ideal gas" contribution, which remains even for infinitely diluted colloidal suspensions. The Smoluchowski equation approach leads to explicit expressions for these virial coefficients in terms of the pair-interaction potential for colloid-colloid interactions and hydrodynamic interaction functions.

For the case of a hard sphere, the pair-interaction potential is temperature independent, so that,

$$\alpha_T^i = 0 \ . \tag{13}$$

A calculation of α_T^0 for the hard-sphere potential then leads to,

$$D_{\rm T,int}^{\rm theo} = D_0 \frac{\rho_{\rm N}}{T}[1 - 0.35\phi + \mathcal{O}(\phi^2)] \ . \tag{14}$$

Hence, from eq. 10, to leading order in colloid concentration,

$$D_{\rm T} = D_{\rm T,int} + D_{\rm T,sing} = \frac{D_0}{T}\frac{1-0.35\phi}{1-\phi} + D_{\rm T,sing} \approx \frac{D_0}{T}(1+0.65\phi) + D_{\rm T,sing} \ , \tag{15}$$

where $D_{\rm T,sing}$ is the single particle contribution to the thermal diffusion coefficient, that is, the diffusion coefficient that one would measure at infinite dilution where colloid-colloid interactions are absent. The single particle contribution $D_{\rm T,sing}$ relates to specific interactions of the colloidal interface and solvent, which is generally temperature dependent. From the well-known leading order concentration dependence of the translational diffusion coefficient $D = D_0(1 + 1.45\phi)$,[24] the Soret coefficient for hard-spheres is thus found to be equal to,

$$S_{\rm T} = \frac{D_{\rm T}}{D} = \frac{1}{T}\frac{1-0.35\phi}{(1-\phi)(1+1.45\phi)} + \frac{D_{\rm T,sing}}{D_0(1+1.45\phi)} \approx \frac{1}{T}(1-0.80\phi) + S_{\rm T,sing}(1-1.45\phi) \ , \tag{16}$$

where $S_{\rm T,sing}$ is the single-particle contribution to the Soret coefficient.

III. EXPERIMENT

A. Synthesis

Silica-core particles were synthesized by the hydrolysis and condensation of tetraethylorthosilicate(TEOS) following Stöber.[25] These particles were rendered organophilic by a grafting procedure with octadecyl alcohol according to van Helden.[26] The dispersion was

purified from the excess octadecyl alcohol by vacuum distillation followed by repeated cycles of centrifugation and re-dispersion, first in chloroform and cyclohexane and then in toluene to prepare the final stock solution with a volume fraction of 10.75%. The concentration of these solutions was determined by drying a small volume of dispersion to constant weight at 50°C, from which the volume fraction of the dispersions was obtained using the density of the particles. The density of the particles was determined from the density of a dispersion with a concentration of 0.186 g cm^{-3}. This was done by weighting 1 cm^3 of the dispersion as well as the solvent toluene. Assuming additivity of volumes of solvent and particles, which is a good assumption for these colloidal dispersions, a density of the particles of ρ=1.73 g cm^{-3} was obtained.

Elemental analysis was performed by the Central Division of Analytical Chemistry (ZCH) of the Forschungszentrum Jülich on a LECO CHNS-932 analyzer. The sample was dried for overnight at 50 °C under vacuum. An average carbon content of 11 wt% was obtained, which is attributed to 13 wt% alkyl chains. However the amount of alkyl chains on the surface might be lower than this value, because of trapping of alkyl chains within the core of the particle.[27]

B. Sample preparation

For TDFRS measurements, the colloidal samples were prepared as follows. For samples with a volume fraction below 10 %, a certain amount of the stock dispersion was diluted by adding toluene, while for the higher concentrated samples, part of the stock dispersion was concentrated by carefully evaporating the toluene under a nitrogen flow. Thirteen different concentrations of colloidal dispersions were prepared. The colloid content varies between 1 % and 30 % in volume. Each solution was filtrated directly into an optical quartz cell with 0.2 mm path length (Hellma) through a 5 μm PTFE membrane filter. The colloidal samples for the TDFRS measurements were always prepared one day before the measurement to deposit the possible dust in the solution.

The thermal diffusive behaviour of octadecane/toluene mixtures was also studied. The octadecane (Aldrich, purity≥99.5 %) and toluene (Fluka, purity≥99.0 %) were used without further purification. The process to prepare a sample for TDFRS measurement is the same as that of the colloidal dispersion.

A trace amount of quinizarin (Aldrich purity 96 %, less than 10^{-4} by weight fraction) is added and used to create a temperature grating by absorption from an optical grating. Absorption spectra were measured with a Carry 50 spectrometer and a rectangular quartz cuvette with a path length of 1 mm (Hellma). Fig.1 shows the absorption curves. Comparing the absorption curves with colloids (solid line) and without colloids (dashed line), one finds no shift of the absorption band to other wavelengths. We can therefore assume that the dye is homogenously distributed in the dispersion and does not adsorb at the colloidal surfaces as in the case of boehmite.[11] The additional apparent absorption at low wavelengths is due to the light scattering of the colloidal particles, which is shown by the spectrum of the colloidal suspension without dye (dotted line). The contribution of the scattered light to the total absorption is around 15% at the wavelength of 488 nm, but it does not influence the prerequisite of the TDFRS experiments (strong absorption at 488 nm, negligible absorption at 632.8 nm).

C. Thermal diffusion forced Rayleigh scattering (TDFRS)

The experimental setup of TDFRS has been described in detail elsewhere.[7,28] In brief, an interference grating was written by an argon-ion laser operating at the wavelength of λ=488 nm. The grating was read out by a He-Ne laser at λ=632.8 nm. The intensity of the diffracted beam was measured with a photomultiplier. The TDFRS measurements were carried out in a temperature range from 15.0 to 50.0 °C. The temperature of the sample cell was thermostatically controlled by circulating water bath with an uncertainty of 0.02 °C.

To calculate the Soret coefficient S_{T} and the thermal diffusion coefficient D_{T} from TDFRS data, the refractive index increments $\partial n/\partial T$ and $\partial n/\partial w$ of the colloidal dispersion are required. These increments are measured separately by using a Michelson interferometer at a wavelength of 632.8 nm.[29] Fig.2 shows the increment $\partial n/\partial T$, measured at different temperatures as a function of the colloid concentration of the dispersion. As can be seen, $\partial n/\partial T$ varies linearly with concentration within the investigated range. In Fig.3, the increment $\partial n/\partial w$ decreases slightly with increasing temperature.

The refractive index increments were also determined for the octadecane/toluene mixture with a weight fraction 5 % octadecane. $\partial n/\partial T$ was found to be equal to $-5.51 \cdot 10^{-4}$, $-5.52 \cdot 10^{-4}$, $-5.54 \cdot 10^{-4}$, $-5.57 \cdot 10^{-4}$ and $-5.59 \cdot 10^{-4}$ K^{-1} for 15, 20, 30, 40 and 50 °C,

respectively, and $\partial n/\partial w$ is equal to -0.076.

In the TDFRS experiment, the heterodyne signal intensity of the read out laser is proportional to the amplitude of the refractive index gradient $\Delta n\,(T, w)$ as,[29]

$$\Delta n\,(T, w) = \left(\frac{\partial n}{\partial T}\right) \Delta T + \left(\frac{\partial n}{\partial w}\right) \Delta w\ . \tag{17}$$

The normalized total intensity $\zeta_{\rm het}\,(t)$ to the thermal signal is related to the Soret coefficient as,

$$\zeta_{\rm het}\,(t) = 1 + \left(\frac{\partial n}{\partial T}\right)^{-1} \left(\frac{\partial n}{\partial w}\right) S_{\rm T} w\,(1-w) \left(1 - e^{-q^2 D t}\right)\ . \tag{18}$$

The Soret coefficient $S_{\rm T}$ in eq.18 is defined as the Soret coefficient of component 1. A positive sign of $S_{\rm T}$ implies that component 1 moves to the cold side.

D. Dynamic light scattering (DLS)

Dynamic light scattering (DLS) was carried out in the angular range $30^\circ < \theta < 135^\circ$ with a Kr-ion laser (wavelength λ = 647.1 nm). An ALV-5000E correlator was used to measure the auto correlation function. The samples for the DLS experiment were prepared and cleaned in the same way as those for the TDFRS measurements and filtered directly into a cylindrical cell with an inner diameter of 8.5 mm. The sample cell was placed in a thermostated bath with a temperature uncertainty of 0.1 °C. Before data acquisition we stabilized the sample cell for at least 30 minutes.

The measured auto correlation function of the scattered light intensity $g^{(2)}\,(q, t)$ is related to the normalized field correlation function $g^{(1)}\,(q, t)$ through the Siegert relation,

$$g^{(2)}\,(q, t) = B\left(1 + \beta[g^{(1)}\,(q, t)]^2\right)\ , \tag{19}$$

where B and β are the baseline and a constant related to the coherence of detection, respectively. Measured correlation functions were fitted to a second cumulant approximation,

$$\ln g^{(1)}\,(t) = -\bar{\Gamma} t + \frac{\mu_2}{2!} t^2\ , \tag{20}$$

where $\bar{\Gamma}$ is the decay rate and μ_2 is the second cumulant. The second cumulant accounts for the polydispersity of the colloids : $\mu_2/\bar{\Gamma}^2$ equals the relative standard deviation of the size of the colloids. If the fluctuation of the scattering light intensity is due to the translational

diffusion motion of colloids, the decay rate is related to the mass diffusion coefficient D as,

$$D = \lim_{q \to 0} \bar{\Gamma}/q^2 \ . \tag{21}$$

For the small colloidal spheres studied in the present paper, the asymptotic value for the collective diffusion coefficient for small wave vectors q is attained for all scattering angles. For the sticky-sphere potential in Eq.3, the mass diffusion coefficient D is related to the interaction parameters as given by Eq.8. This allows to determine interaction parameters by dynamic light scattering.

For very small colloid concentrations, D is equal to the Stokes-Einstein diffusion coefficient $D_0 = k_{\rm B}T/6\pi\eta_0 R_{\rm h}$ (with η_0 the shear viscosity of the solvent and $R_{\rm h}$ the hydrodynamic radius of a colloidal sphere), which allows for the characterization of the (average) colloid-particle size.

E. Static light scattering (SLS)

Static light scattering (SLS) was carried out in the angular range $30^\circ < \theta < 150^\circ$ with a Helium-Neon laser (632.8 nm, $P = 20$ mW). The cylindrical quartz cells had a diameter of 2 cm. The temperature stability and filtering procedure was the same as in the DLS experiment. Data were corrected for solvent background and converted into Rayleigh ratios as follows,

$$\Delta R_\theta = \frac{I_{\rm solution} - I_{\rm tol}}{I_{\rm tol}} \left(\frac{n_{\rm solv}}{n_{\rm tol}} \right)^2 R_{\rm tol} \tag{22}$$

where $I_{\rm solution}$ and $I_{\rm tol}$ denote the scattered intensities corresponding to solution and toluene reference, respectively. $n_{\rm solv}$ and $n_{\rm tol}$ denote the refractive index of solvent and toluene. The Rayleigh ratio of toluene was taken to be $R_{\rm tol} = 1.3526 \times 10^{-5}$ cm^{-1}. We investigated six concentrations between $c = 0.58$ and 4.29 g/L. Scattering data were analyzed using the linear approximation by a Zimm plot,

$$\frac{Kc}{\Delta R_\theta} = \frac{1}{M_{\rm w}} \left(1 + \frac{q^2 {R_{\rm g}}^2}{3} \right) + 2A_2 c \ , \tag{23}$$

where $K = 2\pi^2 n^2 (\partial n/\partial c)^2/\lambda_0^4 N_{\rm A}$ and c is the colloid concentration in g/L. $R_{\rm g}$ the radius of gyration. A_2 is the second virial coefficient, which relates to the leading virial coefficient B_2 for the osmotic pressure as,

$$B_2 = A_2 M_{\rm W}^2 / N_{\rm A} \ , \tag{24}$$

where $M_{\rm W}$ is the mass and $N_{\rm A}$ is Avogadro's constant.

IV. RESULTS

A. Characterization and phase behaviour of the colloidal dispersion

Fig.4a shows the TEM image of the investigated colloidal particles. It is obvious that the particles are not perfectly spherical. The size distribution of the radius is displayed in Fig.4b. This distribution renders and number-average radius of $< R_{\mathrm{TEM}} >$=14.3±5.8 nm.

Additionally we performed DLS measurements to characterize the colloidal dispersions in the same temperature range as for the TDFRS measurements. The volume fraction of the colloids for DLS measurements is 0.25 %, at which concentration colloid-colloid interactions can be neglected. By analyzing DLS data, colloidal parameters, such as the self diffusion coefficient (D_0), hydrodynamic radius (R_{h}) and the polydispersity index ($\mu_2/\overline{\Gamma}^2$) were obtained, which are shown in Tab.I. The diffusion coefficient D_0 increases with increasing temperature, which is due to the decrease of the viscosity. The average hydrodynamic radius $< R_h >$ is found to be temperature independent $< R_{\mathrm{h}} >= 26.5 \pm 0.4$nm. This result deviates significantly from $< R_{\mathrm{TEM}} >$. The difference can be understood by the different statistical weights in obtaining averages from the two methods. For DLS, the contribution to the measured scattered intensity of each colloidal particle proportional to its volume squared. Hence, for a polydisperse system the large colloidal particles will contribute significantly more to the detected scattered intensity. The radius obtained from TEM pictures, however, is a number-averaged value. One can calculate the number-averaged radius R_N from the DLS result[30] by

$$R_N =< R_h > /(1 + \mu_2/\bar{\Gamma}^2)^5 \tag{25}$$

The calculated R_N in Tab.I shows good agreement with the TEM result.

The phase diagram was measured experimentally by slowly cooling down dispersions with varying concentration. The boundary between stable and turbid phases was measured by observing the sharp decrease of the intensity of a through-going beam, and the gel line was obtained by observing the sample by eye. The obtained phase diagram is shown in Fig.5. In the high temperature regime the dispersion is stable. With decreasing temperatures, the attractive force between the particles increases, and the dispersion becomes turbid. Further cooling down leads to a gel phase for volume fractions above 5 % within the investigated temperature range. Thermal diffusion experiments are always done at the temperature range

at least 15-20 °C higher than the unstable region.

In order to characterize the attractive potential between the colloids, DLS and SLS measurement were performed. DLS measurements were performed for the colloidal dispersion in a concentration range ϕ=1.8-13 % and a temperature range 15-50 °C. As displayed in Fig.6(a), the translational diffusion coefficient increases linearly for all temperatures with increasing volume fraction. With a particle radius of $a = 27$ nm (which is the radius relevant for scattering experiments) and a width of the interaction potential $\triangle$=0.3 nm (which is the thickness of grafted octadecyl layer onto the surfaces of the colloids)[20,23] we determined the attractive potential parameter $\beta\epsilon$ by fitting the data according to Eq.8 for DLS. As can be seen from Fig.6b, $\beta\epsilon$ decreases with decreasing temperature. As expected, the depth of the attractive interaction increases on approach of the gas-liquid phase transition line from the stable region in the phase diagram. With increasing temperature, the attractive potential vanishes, which makes it more difficult to determine $\beta\epsilon$ from dynamic light scattering and leads to large error bars.

Additionally, we performed SLS measurements in order to determine the second virial coefficient. The data were analyzed using the linear approximation by Zimm (Eq.23). The so determined A_2 parameter was converted to B_2 according to Eq.24. The ratio $B_2/V_{\rm HS}$ increases with temperature and reaches the plateau value of 4 for hard spheres at temperatures above about 30 °C (see Fig.6(b)).

The light scattering experiments thus show that attractions can be neglected at temperatures above $30 - 50$ °C.

B. Thermal diffusion measurements

TDFRS measurements were performed in the concentration range between 1 % and 30 % for different temperatures between 15 °C and 50 °C. Typical normalized heterodyne TDFRS signals $\zeta_{\mathbf{het}}(t)$ are displayed as function of time in Fig.7. The volume fraction of the colloidal dispersion is ϕ =10 %. The inset shows the signal measured at 50 °C with a logarithmic time scale. The rapid increase of $\zeta_{\rm het}(t)$ is due to the establishment of the temperature gradient, and the following slower variation reflects the formation of a concentration gradient due to thermal diffusion. The signal $\zeta_{\rm het}(t)$ has been normalized to the thermal plateau. As can be seen, the concentration part of the signal decays at lower temperatures and increases

from higher temperatures. Since $(\partial n/\partial w) > 0$, this implies that the colloids move at low temperatures to the warm and at high temperatures to the cold side.

Fig.8 presents the Soret coefficient and the thermal diffusion coefficient as a function of the volume fraction at various temperatures. Both S_{T} and D_{T} show a weak concentration dependence in the low concentration regime, while a pronounced decrease is observed in the high concentration regime. As can be seen there is a sign change with increasing concentrations at $T = 30$ °C and $T = 40$ °C. The errors displayed in Fig.8(a) correspond to one standard deviation. High uncertainties occur for low concentrations, where the amplitude of the concentration part of the signal is rather small.

The Soret coefficient S_{T} and the thermal diffusion coefficient D_{T} versus temperature are plotted in Fig.9 for various concentrations. Both coefficients increase with increasing temperatures, and the strong temperature dependence eventually leads to a sign change from negative to positive between 30 °C and 45 °C. The sign change temperature $T^{\pm}$ increases with increasing volume fraction (see Fig.10), which might be an indication for a stronger interaction between the colloids. Sign change of the thermal diffusion coefficient with varying temperature has also been found for several other systems, such as PEO in the mixture of water and ethanol,[6] PNiPAM/ethanol solution,[31] SDS , and several bio-macromolecule solutions.[12] In all aqueous systems the Soret coefficient increases with temperature, while for the system PNiPAM/ethanol S_{T} decreases with increasing temperature.

C. Thermal diffusion of free octadecane in toluene

The surfaces of our colloidal particles are grafted with octadecyl chains. The interface between the colloidal material, the octadecyl brush, and pure solvent is probably the dominant factor for thermal diffusion of single colloidal particles.[32,33] In order to get a better insight in the single particle diffusive behavior of the colloids, one might learn from the thermal diffusive behavior of free octadecyl chains dissolved in toluene, which is the solvent used for the colloids. The octadecane concentration is 5 wt%.

As can be seen from Fig.11, the Soret coefficient and thermal diffusion coefficient are negative within the entire temperature range under consideration. Free octadecyl chains therefore tend to migrate to the warm side. For our colloids, however, colloidal particles migrate at high temperatures to the cold side. It thus seems that the confinement of the

octadecyl chains due to grafting has an appreciable effect and/or there are other reasons for a single colloidal particle, independent of the grafted brush, to migrate to the cold side at high temperatures.

V. DISCUSSION

As we have mentioned in Sec.II, the expressions for the Soret coefficient and thermal diffusion coefficient given in Dhont's theory only account for the contributions due to colloid-colloid interactions. To compare the experimental data with theory, the single particle contribution $S_{\mathrm{T,sing}}$ and $D_{\mathrm{T,sing}}$ should be added to these expressions. Since we do not have an analytical expression to calculate the single particle contribution, a comparison with theory can only be based on the concentration dependence at a fixed temperature.

In Fig.8, one can observe a strong concentration dependence for S_{T} and D_{T}. This concentration dependence is related to colloid-colloid interactions. The interaction parameters are independently determined by static and dynamic light scattering experiments. In the investigated temperature range, even at the low temperatures the attractive contributions are still quite weak. As a result, the colloids can be regarded as hard spheres. The solid lines in Fig.8 show the fits of our experimental data to the theoretical expressions Eq.16 and Eq.15, respectively. Fitting was performed in the low concentration range ($\phi < 12$ %). As can be seen, the theory is consistent within experimental error. It should be mentioned that the slope of D_{T} and S_{T} as a function of concentration is rather small, which is, however, in accordance with theory. The slope is so small, that more accurate measurements would be needed to quantitatively confirm the theory. It seems not feasible to do accurate experiments to an extent that the theoretically predicted slope can be verified quantitatively. It would be worthwhile to perform experiments close to the phase transition line, where attractions become important. The concentration dependence for such sticky spheres is expected to be more pronounced as compared to hard spheres.

In the high concentration regime, for all temperatures, both D_{T} and S_{T} of the colloids decrease markedly with increasing concentration. The decrease of D_{T} and S_{T} at high concentrations was also observed by Rauch *et al.*[15,34] and Zhang *et al.*[35] for the Polystryrene/toluene solution. In Rauch's work, the decay of D_{T} with concentration was interpreted by the increase of the local viscosity, which is due to the approaching of the glass transition. In our

case the drop of S_T and D_T might have a similar reason, because at the higher concentrations we are closer to the gelation boundary. In Fig.8(a), we observe for concentrated dispersions ($\phi > 15$ %) that S_T follows a scaling law $S_T \propto \phi^{-0.0095} \propto c^{-0.0095}$ for all temperatures. Compared to the scaling law $S_T \propto C^{-1.0}$ for polystryrene/toluene, the exponent is two orders of magnitudes smaller.

The single particle contributions $S_{T,sing}$ and $D_{T,sing}$ as obtained from the fit are plotted in Fig.12. From this figure one can see that the single particle contribution to D_T and S_T increases with temperature and changes sign from negative to positive. The single particle contribution is probably mainly determined by the interface interaction between the colloid and solvent.[32,36–38] Duhr and Braun[38] showed for diluted solutions of DNA and polystyrene beads that the solvation layer is one main contribution to the single-particle Soret coeffcient, and that the contribution from the colloidal bulk-material is much less important. It seems therefore appropriate to compare our results to the thermal diffusion behavior of the surface material, octadecane, in toluene. Comparing the Soret coefficient S_T of octadecane (see Fig.11(a)) with $S_{T,sing}$, we find that both parameters increase with temperature, however in the studied temperature range S_T of octadecane is negative and does not change sign.

Fig.9 shows that the thermal diffusion behavior of the studied colloidal system has a strong dependence on the temperature. At low temperatures the colloids move to the warm side, while at high temperature the colloids prefer the cold side. Increasing the temperature improves the solvent quality, while at low temperatures we are closer to poor solvent conditions. Also for polymers it was observed by experiment,[39,40] simulations[41] and by lattice model calculations,[42] that under poor solvent conditions the solutes tend to accumulate in the warm region. Both S_T and D_T increase with the temperature. The linear temperature dependence of D_T that is found seems to be quite universal for many systems and was interpreted by a semi-empirical expression $D_T = A(T - T^{\pm})$, where $T^{\pm}$ is the sign-change temperature and A is a system-dependent amplitude.[12] Sometimes the temperature dependence of D_T is related to the thermal expansion coefficient of solvent,[12,43] but there is no quantitative theory to predict the amplitude.

Since the thermal diffusion behavior of the colloidal system consist of a single and a colloid-colloid interaction part, and both contributions depend on the temperature, it is worth to investigate the two effects separately. While the colloid-colloid interaction part of S_T and D_T displayed in Fig.12 is almost temperature independent, the single parts show

a pronounced increase with temperature. Therefore, we conclude that the temperature dependence is mainly caused by the single particle contribution.

For all investigated concentrations we observed a sign change with temperature. Although a sign change with temperature and concentration has also been predicted by the theory of Dhont,[9] the physical origin might be different in our case. As we have seen, our system is close to a hard sphere system, so that the observed sign change with temperature is not caused by a temperature dependence of the interaction potential between the colloidal particles, but is probably a single particle contribution. This hypothesis is supported by our study of octadecane in toluene, which shows also a pronounced temperature dependence (see Fig.11), although we could not observe a sign change in the investigated temperature range. Therefore, we conclude that sign change of S_{T} and D_{T} of the studied colloidal system with temperatures is not caused by varying attraction between the particles but due to changes of the colloidal interface structure.

VI. CONCLUSION

The thermal diffusion behavior of alkyl coated spherical colloidal particles dispersed in toluene presents a pronounced dependence on both concentration and temperature. At low temperatures the colloidal particles tend to concentrate on the warm side ($S_{\mathrm{T}} < 0$), while the colloids migrate to the cold side at higher temperatures ($S_{\mathrm{T}} > 0$). With increasing concentration the sign change temperature also increased. We can conclude, that the solvent conditions are better at higher temperatures. The observation that the solute particles move to the cold side under good solvent conditions is in agreement with previous studies.[40,41]

According to the light scattering measurement and the phase diagram, we know that the attractive potential increases with decreasing temperature. However in the studied temperature range, the colloids exhibit predominantly hard sphere behavior. Due to experimental limitations like the occurence of condensation, lower temperatures can not be reached and therefore the range of strong attractions is unaccessible. Strongly attractive colloids will be studied in the future with a similar system but with different coating density, rendering the phase transition line at higher temperatures.

The experimental results are compared with the theory by Dhont for hard spheres, where the single particle contribution is treated as a fitting parameter. In the intermediate concen-

tration range we found a weak concentration dependence of the thermal diffusion coefficient, in accordance with theory. The effects of temperature are dominated by the single particle contribution, for which there is not a suitable theory available yet.

Single particle thermal diffusion was studied by investigating the thermal diffusion of the coating material in toluene. It turns out that octadecane in toluene shows a strong temperature dependence, but no sign change occurs in the investigated temperature range. This is an indication that other effects influence the thermal diffusion behavior. There might be contributions from the silica core of the particles, or the fact that octadecane is bound to a surface or an effect which depends on the octadecane concentration. In general one can expect, that if the particle coating changes from "organophilic" to "organophobic" a sign change could be expected, but under which conditions this is the case needs to be clarified in further investigations.

APPENDIX: CONVERSION OF D_T^{theo} TO D_T

The experimentally determined D_T need to be converted for comparison with the theory by Dhont.[9] Dhont defines D_T^{theo} by the following flux equation,

$$\frac{\partial}{\partial t}\rho_N = D\nabla^2\rho_N + D_T^{theo}\nabla^2 T \ , \tag{A.1}$$

where ρ_N=N/V is the number density of the colloids. N and V are total number of colloids and the volume respectively.

Experimentally, the fitting function for the TDFRS heterodyne signal is derived from,

$$\frac{\partial w}{\partial t} = D\nabla^2 w + w(1-w)D_T\nabla^2 T \ , \tag{A.2}$$

which is equal to,

$$\frac{\partial \phi}{\partial t} = D\nabla^2 \phi + \phi(1-\phi)D_T\nabla^2 T \ , \tag{A.3}$$

where the w and ϕ are weight fraction and volume fraction respectively. The volume fraction can be obtained by,

$$\phi = V_c^0 \cdot \frac{N}{V} \ , \tag{A.4}$$

where the V_c^0 is the geometric volume of a single colloidal particle. The mass conservation equation Eq.A.1 can thus be written as,

$$V_c^0 \cdot \frac{\partial \rho_N}{\partial t} = V_c^0 D\nabla^2\rho_N + V_c^0 D_T^{theo}\nabla^2 T \ , \tag{A.5}$$

that is,

$$\frac{\partial \phi}{\partial t} = D\nabla^2\phi + V_c^0 D_{\rm T}^{\rm theo}\nabla^2 T \ . \tag{A.6}$$

Comparison of Eq.A.6 and Eq.A.3 yields,

$$D_{\rm T} = \frac{V_c^0 D_{\rm T}^{\rm theo}}{\phi(1-\phi)} \ . \tag{A.7}$$

Actually, $D_{\rm T}^{\rm theo}$ contains two contributions

$$D_{\rm T}^{\rm theo} = D_{\rm T,int}^{\rm theo} + D_{\rm T,sing}^{\rm theo}, \tag{A.8}$$

where $D_{\rm T,int}^{\rm theo}$ originates from colloid-colloid interactions and $D_{\rm T,sing}^{\rm theo}$ is the single particle contribution. Theory predicts that for hard spheres,

$$D_{\rm T,int}^{\rm theo} = D_0\frac{\rho_{\rm N}}{T}(1-0.35\phi) \ , \tag{A.9}$$

to leading order in volume fraction. If we replace the $D_{\rm T}^{\rm theo}$ in Eq.A.7 by Eq.A.8 and Eq.A.9, we obtain,

$$D_{\rm T} = \frac{D_0\rho_{\rm N}V_c^0}{\phi(1-\phi)T}(1-0.35\phi) + D_{\rm T,sing} = \frac{D_0(1-0.35\phi)}{T(1-\phi)} + D_{\rm T,sing} \ . \tag{A.10}$$

Hence,

$$D_{\rm T} \ = \ \frac{D_0}{T}(1+0.65\phi) + D_{\rm T,sing} \ , \tag{A.11}$$

again to leading order in volume fraction.

ACKNOWLEDGMENTS

The authors would like to thank Hartmut Kriegs and Pavel Polyakov for their experimental assistance. The help of Beate Müller and Christine Rosenauer from MPI for polymer research for their assistence in the static light scattering experiments. We thank Peter Lang, Pavlik Lettinga, Remco Tuinier and Zhenkun Zhang for their valuable discussions. This work was partially supported by the Deutsche Forschungsgemeinschaft grant Wi 1684.

* h.ning@fz-juelich.de; http://www.fz-juelich.de/iff/personen/H.Ning/

† j.buitenhuis@fz-juelich.de; http://www.fz-juelich.de/iff/personen/J.Buitenhuis/

‡ J.K.G.Dhont@fz-juelich.de; http://www.fz-juelich.de/iff/personen/Dhont_J_K_G/

§ s.wiegand@fz-juelich.de; http://www.fz-juelich.de/iff/personen/S.Wiegand/

[1] C. Ludwig, Sitz. ber. Akad. Wiss. Wien Math.-naturw. Kl **20**, 539 (1856).

[2] C. Soret, Arch. Geneve **3**, 48 (1879).

[3] R. Piazza, Philos. Mag. **83**, 2067 (2003).

[4] K. Morozov, J. Magn. Magn. Mater. **201**, 248 (1999).

[5] S. A. Putnam and D. G. Cahill, Langmuir **21**, 5317 (2005).

[6] R. Kita, S. Wiegand, and J. Luettmer Strathmann, J. Chem. Phys. **121**, 3874 (2004).

[7] H. Ning, R. Kita, H. Kriegs, J. Luettmer-Strathmann, and S. Wiegand, J. Phys. Chem. B. **110**, 10746 (2006).

[8] J. K. G. Dhont, J. Chem. Phys. **120**, 1632 (2004).

[9] J. K. G. Dhont, J. Chem. Phys. **120**, 1642 (2004).

[10] M. E. Schimpf and S. N. Semenov, J. Phys. Chem. B **104**, 9935 (2000).

[11] B. J. de Gans, R. Kita, B. Müller, and S. Wiegand, J. Chem. Phys. **118**, 8073 (2003).

[12] S. Iacopini, R. Rusconi, and R. Piazza, Eur. Phys. J. E **19**, 59 (2006).

[13] S. Duhr, S. Arduini, and D. Brauna, Eur. Phys. J. E **15**, 277 (2004).

[14] S. Duhr and D. Braun, Phys. Rev. Lett. **96**, 168301(1 (2005).

[15] J. Rauch and W. Köhler, Macromolecules **38**, 3571 (2005).

[16] S. Fayolle, T. Bickel, S. Le Boiteux, and A. Würger, Phys. Rev. Lett. **95**, 208301 (2005).

[17] E. Bringuier and A. Bourdon, Phys. Rev. E **67**, 011404 (2003).

[18] A. Parola and R. Piazza, Eur. Phys. J. E. **15**, 255 (2004).

[19] A. Parola and R. Piazza, J. Phys.:Condens. Matter **17**, S3639 (2005).

[20] P. W. Rouw, A. Virj, and C. G. de Kruif, Progr. Colloid Polym. Sci. **76**, 1 (1988).

[21] J. W. Jansen, C. G. De Kruif, and A. Vrij, J. Colloid Interf. Sci. **114**, 481 (1986).

[22] J. W. Jansen, C. G. De Kruif, and A. Vrij, J. Colloid Interf. Sci. **114**, 492 (1986).

[23] H. Verduin and J. K. G. Dhont, J. Colloid Interface Sci. **172**, 425 (1995).

[24] G. Batchelor, J. Fluid Mech. **74**, 1 (1976).

[25] W. Stöber, A. Fink, and E. Bohn, J. Colloid Interf. Sci. pp. 62–69 (1968).

[26] A. K. Vam Helden, J. W. Jansen, and A. Vrij, J. Colloid Interf. Sci. **81**, 354 (1981).

[27] J. Kohlbrecher, J. Buitenhuis, J. Meier, and M. P. Lettinga, J. Chem. Phys. **accepted** (2006).

[28] S. Wiegand, J.Phys.:Condens. Matter **16**, R357 (2004).

[29] W. Köhler and R. Schäfer, in *New Developments in Polymer Analytics Ii*, edited by M. Schmidt (Springer, Berlin, 2000), vol. 151 of *Advances in Polymer Science*, pp. 1–59.

[30] J. C. Thomas, J. Colloid Interf. Sci. **117**, 187 (1987).

[31] R. Kita, G. Kircher, and S. Wiegand, J. Chem. Phys. **121**, 9140 (2004).

[32] P. M. Shiundu and J. C. Giddings, J. Chromatogr. A **715**, 117 (1995).

[33] P. M. Shiundu, P. S. Williams, and J. C. Giddings, J. Chromatogr. A **715**, 117 (1995).

[34] J. Rauch and W. Köhler, Phys. Rev. Lett. **88**, 185901 (2002).

[35] K. J. Zhang, M. E. Briggs, R. W. Gammon, J. V. Sengers, and J. F. Douglas, J. Chem. Phys. **111**, 2270 (1999).

[36] S. J. Jeon, M. E. Schimpf, and A. Nyborg, Anal. Chem. **69**, 3442 (1997).

[37] S. Alves, G. Demouchy, A. Bee, D. Talbot, A. Bourdon, and A. M. F. Neto, Philos. Mag. **83**, 2059 (2003).

[38] S. Duhr and D. Braun, Proc. Natl. Acad. Sci. USA (2006), accepted.

[39] M. Giglio and A. Vendramini, Phys. Rev. Lett. **38**, 26 (1977).

[40] B.-J. de Gans, R. Kita, S. Wiegand, and J. Luettmer Strathmann, Phys. Rev. Lett. **91**, 245501 (2003).

[41] M. M. Zhang and F. Müller-Plathe, J. Chem. Phys. (2006), accepted.

[42] J. Luettmer-Strathmann, Int. J. Thermophys. **26**, 1693 (2005).

[43] J. R. Bielenberg and H. Brenner, Physica. A **356**, 279 (2005).

TABLES

TABLE I: Temperature dependence of characteristic parameters for colloid/toluene dispersions. The parameters were obtained by DLS using a volume fraction of colloids around 0.25%.

T (°C)	$< D_0 >$ / by extrapolation ($10^{-7} cm^2 s^{-1}$)	$< R_{\rm h} >$ (nm)	$\mu_2/\bar{\Gamma}^2$	R_N (nm)
15.0	1.30 / 1.38	26.5	0.12	15.0
20.0	1.39 / 1.49	26.5	0.11	15.7
30.0	1.61 / 1.70	26.7	0.13	14.5
40.0	1.85 / 1.85	26.5	0.13	14.3
50.0	2.05 / 2.20	27.4	0.15	13.6

LIST OF FIGURES

contribution (⊞) as function of temperature. (b) Shows the corresponding plot for the thermal diffusion coefficient. The volume fraction of the colloidal dispersion is $\phi = 10$ %. The solid lines are linear fits to the data.

FIGURES

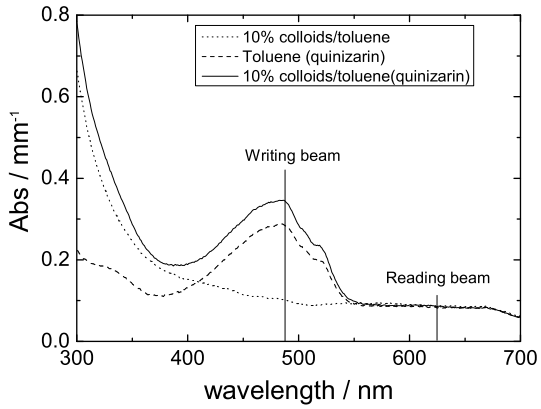
10% colloids/toluene
Toluene (quinizarin)
10% colloids/toluene(quinizarin)
Writing beam
Reading beam
Abs / mm-1
wavelength / nm
0.0
0.2
0.4
0.6
0.8
300
400
500
600
700

FIG. 1:

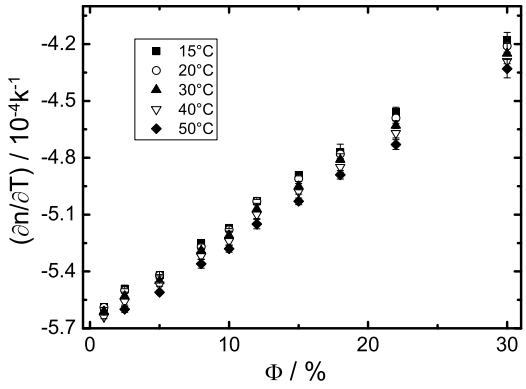

FIG. 2:

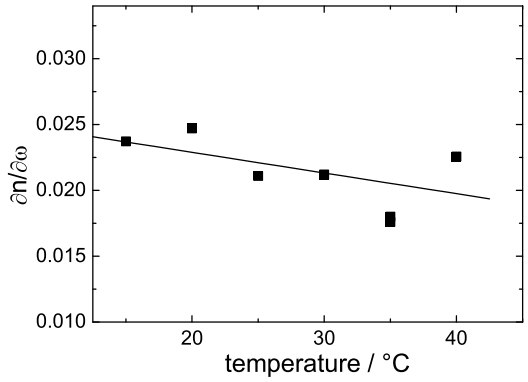

FIG. 3:

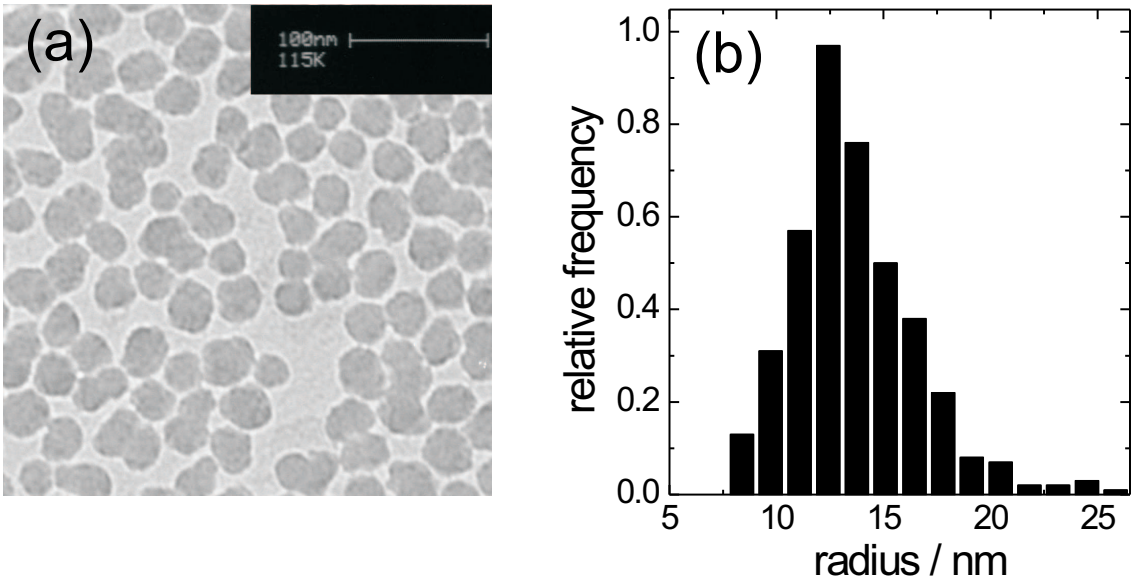
(a)
100nm
115K
(b)
relative frequency
1.0
0.8
0.6
0.4
0.2
0.0
5
10
15
20
25
radius / nm

FIG. 4:

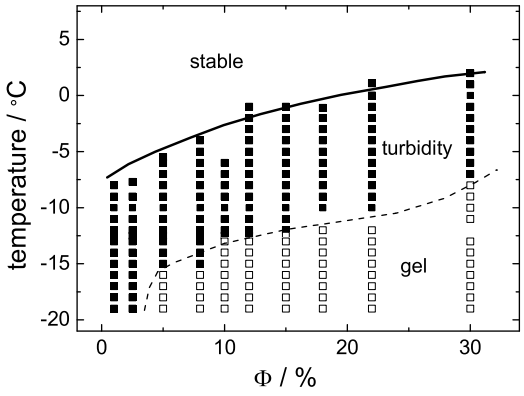

FIG. 5:

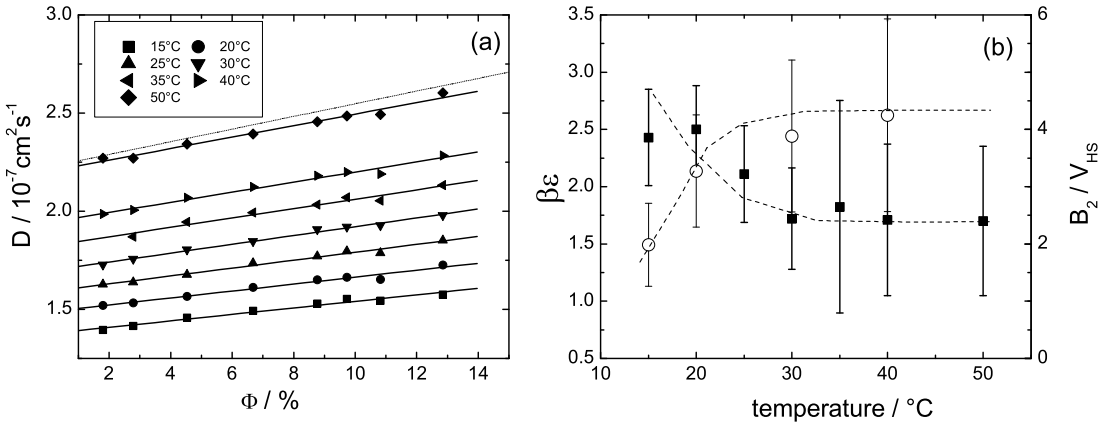
(a)
15°C
20°C
25°C
30°C
35°C
40°C
50°C
D / 10^-7 cm^2 s^-1
Φ / %
(b)
βε
B2 / VHS
temperature / °C

FIG. 6:

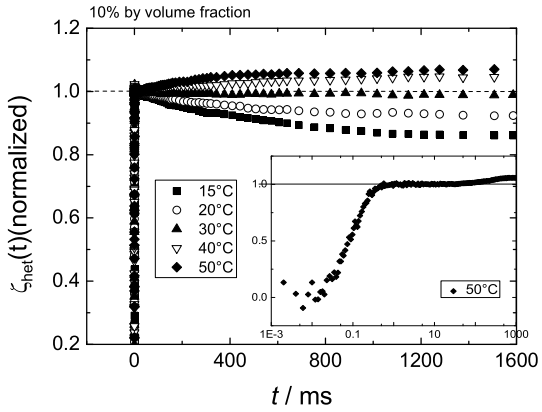
10% by volume fraction
1.2
1.0
0.8
0.6
0.4
0.2
$\zeta_{het}(t)$(normalized)
0
400
800
1200
1600
t / ms
15°C
20°C
30°C
40°C
50°C
1.0
0.5
0.0
1E-3
0.1
10
1000
50°C

FIG. 7:

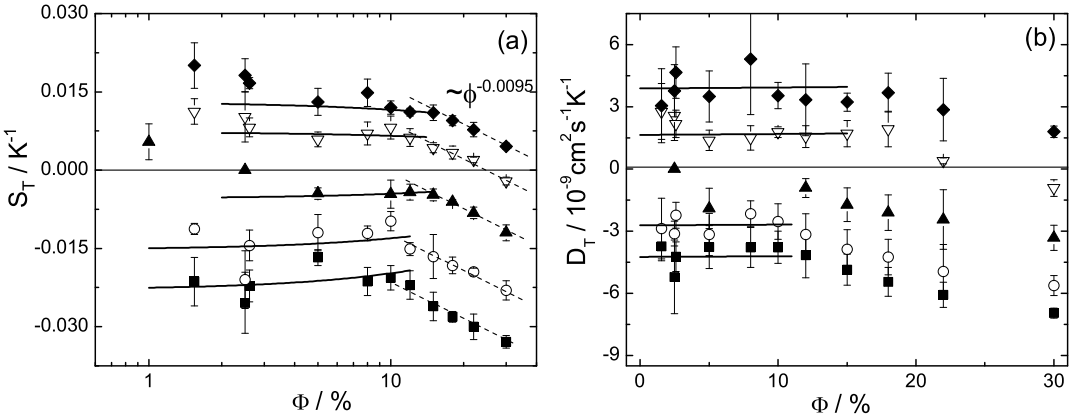
(a)
(b)
S_T / K^{-1}
D_T / 10^{-9}cm^{2}s^{-1}K^{-1}
Φ / %
Φ / %
~ φ$^{-0.0095}$
0.030
0.015
0.000
-0.015
-0.030
1
10
6
3
0
-3
-6
-9
0
10
20
30

FIG. 8:

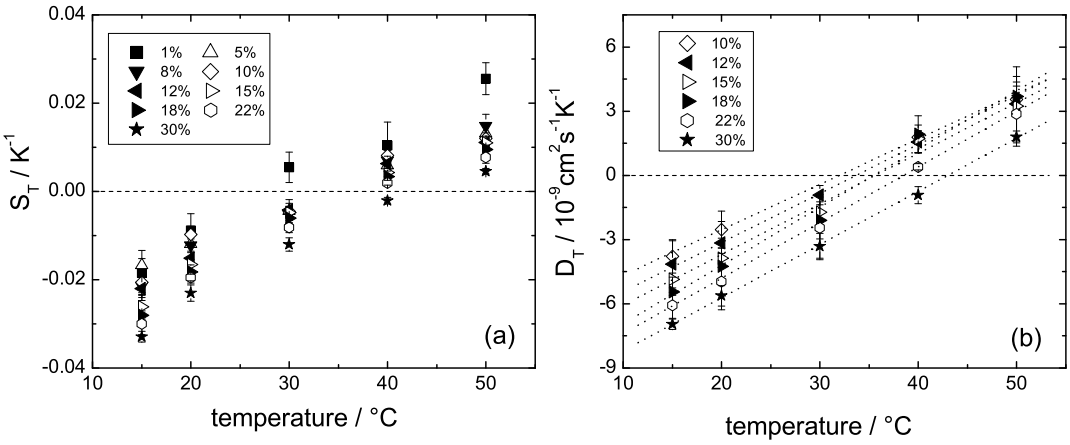
0.04
0.02
0.00
-0.02
-0.04
S_T / K^{-1}
1%
5%
8%
10%
12%
15%
18%
22%
30%
(a)
10
20
30
40
50
temperature / °C
6
3
0
-3
-6
-9
D_T / $10^{-9}cm^2s^{-1}K^{-1}$
10%
12%
15%
18%
22%
30%
(b)
10
20
30
40
50
temperature / °C

FIG. 9:

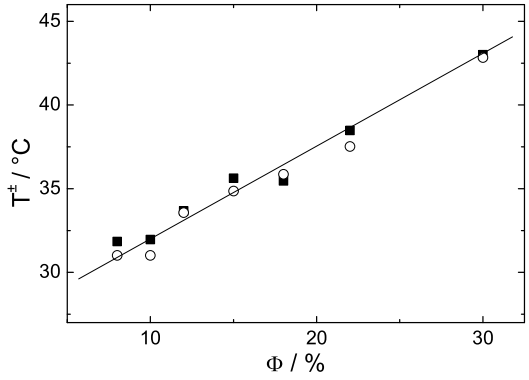

FIG. 10:

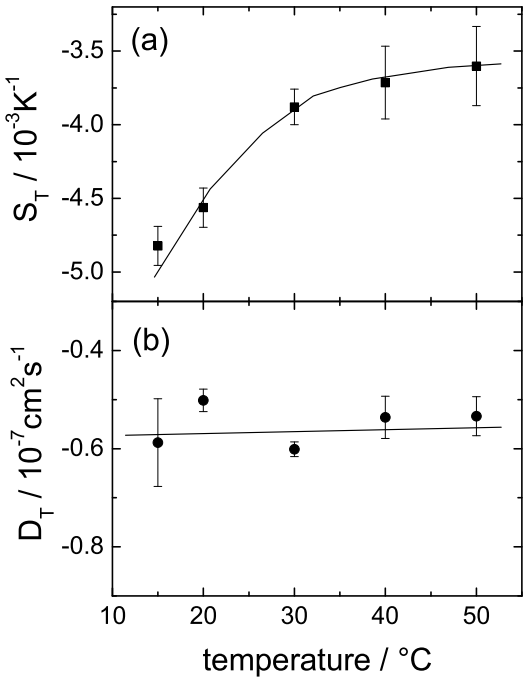
(a)
(b)
S_T / $10^{-3}K^{-1}$
D_T / $10^{-7}cm^2s^{-1}$
-3.5
-4.0
-4.5
-5.0
-0.4
-0.6
-0.8
10
20
30
40
50
temperature / °C

FIG. 11:

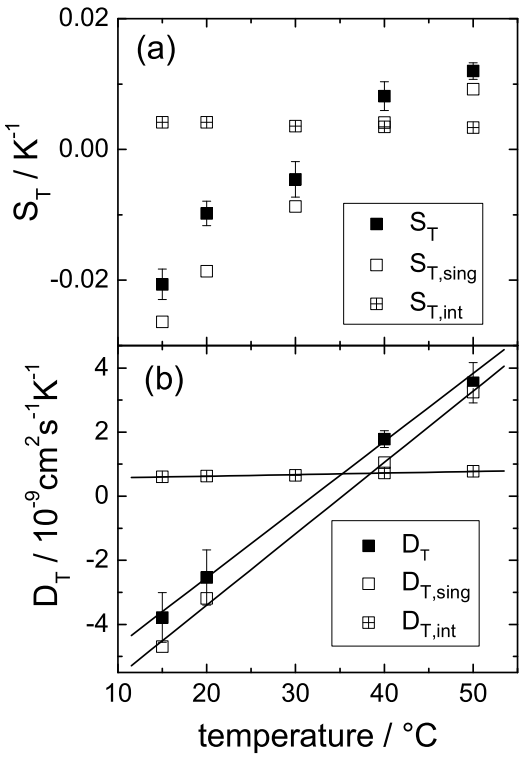
(a)
(b)
S_T / K^{-1}
D_T / $10^{-9}cm^2s^{-1}K^{-1}$
temperature / °C
S_T
$S_{T,sing}$
$S_{T,int}$
D_T
$D_{T,sing}$
$D_{T,int}$
0.02
0.00
-0.02
4
2
0
-2
-4
10
20
30
40
50

FIG. 12: